Structural changes to resorbable calcium phosphate bioceramic aged *in vitro*

Nazia Mehrban*[a], James Bowen[a], Elke Vorndran[b], Uwe Gbureck[b] and Liam M. Grover[a]
[a]School of Chemical Engineering, University of Birmingham, Birmingham, B15 2TT, UK.
[b]Department for Functional Materials in Medicine and Dentistry, University of Würzburg, Pleicherwall 2, 97070 Würzburg, Germany.

*Corresponding author:
E-mail: nazia.mehrban@googlemail.com
Telephone: 0121 414 3887

Abstract

This work investigates the effect of mammalian cell culture conditions on 3D printed calcium phosphate scaffolds. The purpose of the studies presented was to characterise the changes in scaffold properties in physiologically relevant conditions. Differences in crystal morphologies were observed between foetal bovine serum-supplemented media and their unsupplemented analogues, but not for supplemented media containing tenocytes. Scaffold porosity was found to increase for all conditions studied, except for tenocyte-seeded scaffolds. The presence of tenocytes on the scaffold surface inhibited any increase in scaffold porosity in the presence of extracellular matrix secreted by the tenocytes. For acellular conditions the presence or absence of sera proteins strongly affected the rate of dissolution and the distribution of pore diameters within the scaffold. Exposure to high sera protein concentrations led to the development of significant numbers of sub-micron pores, which was otherwise not observed. The implication of these results for cell culture research employing calcium phosphate scaffolds is discussed.

Keywords

Calcium phosphate, degradation, *in vitro*, porosity, structure

1. Introduction

Current methods of bone repair where natural healing is insufficient in repairing the wound site to its former functionality are subject to problems such as disease transmission [1], tissue availability limitations [2] lengthy operating procedures [3], infections [4], poor integration with native tissue [5] and rejection of tissue [6]. When the natural remodeling process of bone healing [7-8] is insufficient in restoring full functionality surgical methods are applied [9]. However, autografts, allografts and xenografts are all subject to a number of limitations [10-12]. Consequently it is necessary to search for an alternative method of bone replacement and as such significant research effort has been focused on the development of synthetic materials to replace bone [13-14]. Biomaterials required for bone substitution need to match certain criteria exhibited by native bone, such as osteoinductivity and osteoconductivity, low inflammatory response and mechanical integrity [15].

Utilising synthetic hard tissue scaffolds in an attempt to eliminate the risks associated with disease transmission, immunogenicity, long operating procedures and the number of operations is one route of bone repair and regeneration. Materials such as polymers and ceramics have been used extensively for regenerating bone [16]. Ceramics based on calcium phosphates (CaP) are physicochemically similar to the mineral component of native bone [9] and have previously been used to engineer bone tissue [17-20] by using ceramics as graft material [21-23]. It is the favourable cellular response both *in vitro* and *in vivo* which has prompted the use of a variety of CaPs such as hydroxyapatite (HA, $Ca_5(PO_4)_3OH$), brushite (dicalcium phosphate dihydrate, $CaHPO_4.2H_2O$) and tricalcium phosphate (TCP, $Ca_3(PO_4)_2$) as potential bone replacement materials. Brushite forms at pH < 4.2 in aqueous solution from the reaction of TCP, in this case β-TCP, with an acidic source of phosphate ions such as phosphoric acid, and exhibits a higher resorption rate than HA under physiological conditions due to poor fluid exchange within the ceramic pores and the low inherent solubility of HA [24-26]. Through a dissolution and reprecipitation process brushite has been shown to eventually form HA.

Computer-aided manufacturing techniques for the production of bespoke scaffolds, such as rapid prototyping, are becoming increasingly popular due to the accuracy in producing grafts according to computer aided design (CAD) images specific to the patient's wound and the ease of manufacture afforded by rapidly printing large quantities [27-29]. These methodologies, namely 3D printing, fused deposition modelling, 3D plotting and indirect rapid prototyping [30] involve the use of CAD to develop complex 3D structures layer by layer. 3D production methods such as fused deposition modelling, resin-curing stereolithography and selective laser sintering require heat and ultraviolet mediated-fusion which cause protein denaturation within the scaffold and do not allow hydrated compounds, such as brushite, to be formed. The layer by layer 3D printing method allows custom design, precision manufacture and the ability to include biological materials such as growth factors [31] within specified regions of the fabricated structure. Furthermore, the printing process is a quick-setting reaction leading to rapid hardening of the scaffold, unlike hand-moulded cements which take considerably longer to set. Klammert *et al*. [32] reported the use of 3D powder printing for the formation of magnesium ammonium phosphate, struvite, for bone replacement specifically with the intention of keeping the pH of the fabricated structures as close to pH 7 as possible. Whilst Vorndran *et al*. [33] have shown that 3D printing technology can be adapted to produce macroporous ceramic structures with localised delivery of bioactive drugs and proteins.

Ageing of brushite-based cements in phosphate buffered saline (PBS) and serum has also been studied [34]. It was found that cements aged in foetal bovine serum (FBS) lost 7 times more weight than those aged in PBS due to the formation of the more stable HA in PBS samples. Since FBS is rich in proteins, polypeptides, amino acids, hormones, glucose, and other nutrients [35] it mimics *in vivo* conditions when added to cell culture media. In particular, it has been suggested that the ligand-receptor activities

which are activated by growth factors within the serum and this influences cellular attachment during *in vitro* studies [36-39].

The current study focuses on characterising the degradation of 3D printed CaP scaffolds during their immersion in a range of aqueous solutions chosen to mimic the *in vitro* and *in vivo* environments. The 3D printed CaP provides an initial condition from which to perform a systematic study such as the one presented here; this is only possible because of the reproducible compositions and microstructures afforded by the 3D printing process. Scaffold manufacture requires the use of H_3PO_4 solution to facilitate rapid setting, followed by further hardening during immersion in H_3PO_4 solution, resulting in a material that is a blend of brushite and monetite, as reported by Mehrban *et al*. [40]. It was found that bespoke scaffold geometries could be formed in this way to 95 ± 0.1 % dimensional accuracy of their original computer-aided design, yielding cements with highly reproducible structures. Samples produced by this technique are therefore suitable for use in systematic evaluations of the stability and/or degradation of synthetic CaPs under clinically relevant conditions.

The aim of this study is to investigate the time-dependent physical and chemical properties of 3D printed synthetic CaPs during prolonged immersion in environments which mimic *in vivo* conditions. A range of environments were employed for these studies: (i) three commonly used mammalian cell culture media, (ii) cell culture media supplemented with FBS, (iii) solutions containing FBS at different concentrations, and (iv) tendon fibroblast (tenocyte) suspensions in FBS-supplemented cell culture media. The results of this study will be of benefit to researchers who wish to use synthetic CaPs *in vitro* and *in vivo*.

2. Experimental

2.1 3D powder printing

Tricalcium phosphate (TCP) was synthesised by heating an equimolar mixture of dicalcium phosphate anhydrous (DCPA, $CaHPO_4$ monetite) (Merck, Darmstadt, Germany) and calcium carbonate (CC, $CaCO_3$, calcite) (Merck, Darmstadt, Germany) to a temperature of 1400 °C for 14 h followed by quenching to room temperature. The sintered cake was crushed with a pestle and mortar and passed through a 160 µm sieve. Milling was performed in a planetary ball mill (PM400, Retsch, Germany) at 200 rpm with 500 mL agate jars, 4 agate balls with a diameter of 30 mm and a load of 125 g TCP per jar for 30 mins. Cement samples were printed with a 3D-powder printing system (Spectrum Z510, Z-Corporation, USA) using the TCP powder and a binder solution of 2.5M phosphoric acid (20 % v/v, Merck, Darmstadt, Germany) as shown in Fig. 1 with a nominal layer thickness of 125 µm, a binder/volume ratio of 0.371 and an isotropic pixel scaling x=y=z= 1.0. Structural geometries were designed using thinkdesign 2007 software (Fa. Think3, Italy) employing discs of mean height 3 mm and mean diameter 16 mm. After printing, any residual loose powder remaining on the sample surfaces was removed using compressed air, followed by hardening via triplicate immersion in 20 % v/v phosphoric acid solution for 30 s per immersion.

2.2 Scanning electron microscopy

To evaluate internal microstructure, the samples were first vacuum dried and sputter coated (Polaron SC7640 sputter coater, UK). For cellular CaP scaffolds, samples were first fixed using 2.5 % v/v glutaraldehyde in 0.1 M PBS for 1 h, followed by dehydration using graded EtOH:H_2O mixtures (50 %, 70 %, 90 %, 100 % EtOH, all v/v) for 30 min each. The samples were then critical point dried by immersion in liquid CO_2 at 1,070 psi and 31 ^{o}C for 60 min. The cement fracture surfaces were Au coated using a SC7640 sputter coater (Polaron, UK). Surfaces were examined using a JEOL JSM 6060 LV scanning electron microscope (SEM) (Oxford Instruments, UK) at an accelerating voltage of 20 kV and a working distance of 10 mm.

2.3 Surface topography

Interferometric measurements for surface roughness of CaP scaffolds were performed using a MicroXAM2 interferometer (Omniscan, UK), operating using a white light source. Samples were first coated with Au using a SC7640 sputter coater (Polaron, UK) to enhance reflectivity and imaged at 10X magnification, acquiring images in a 4x4 grid stitched array, with 45 % overlap between images in order to maximise pixel collection efficiency. The stitched image had dimensions of 2.28 mm x 1.69 mm. Scanning Probe Image Processor software (Image Metrology, Denmark) was employed for the analysis of acquired images, yielding S_a and S_q values for surface roughness.

2.4 Porosity

Disc porosities, ε, were calculated using Eq. 1, where ρ_{app} is the apparent density of the scaffold and ρ_{true} is the true density of the scaffold. Apparent densities were calculated from geometrical measurements taken using a digital caliper (Mitutoyo, UK) and the dry mass of the discs measured using a microbalance (Model 1702 microbalance, Sartorius, UK), after vacuum drying in a vacuum freeze-drier (Edwards EF03 freeze dryer, High Vacuum Ltd., Crawley, UK) for a minimum of 12 h. The uncertainty in the dimensions measured using the digital caliper was ± 10 µm. True densities were determined using a helium pycnometer (AccuPyc II 1340, Micromeritics, UK) employing 100 measurements per sample with overall 5 samples measured per experiment.

$$\varepsilon = 100\left(1 - \frac{\rho_{app}}{\rho_{true}}\right) \quad (1)$$

2.5 Mercury porosimetry

CaP samples were dried overnight in a freeze dryer (Edwards EF03, High Vacuum Ltd., UK), weighed and added to a 3 mL bulb volume glass penetrometer suitable for solid samples. The penetrometer was sealed and the sample analysed using an AutoPore IV mercury porosimeter (Micromeritics, UK) at pressures in the range 3 kPa - 207 MPa. Hg intrusion into the pores of the CaP sample was analysed using the Washburn equation (Eq. 2) in order to determine the pore diameter distribution;

$$D = -\frac{4\gamma}{P}\cos\theta \qquad (2)$$

where D is pore diameter, P is the applied pressure, γ is the surface tension of Hg at 20 °C, which is assumed to be 0.485 N/m, and θ is the contact angle between the Hg and the porous solid, which is assumed to be 130 °.

2.6 X-ray diffraction

X-ray diffraction (XRD) patterns of samples were recorded using monochromatic CuKα radiation (D5005, Siemens, Karlsruhe, Germany). Data were collected from 2θ = 20-40 ° with a step size of 0.02 ° and a normalized count time of 1 s/step. The phase composition was checked by means of reference patterns for ß-TCP and monetite available from the Joint Committee on Powder Diffraction Standards.

2.7 Tenocyte isolation and culture

200 g Wistar male rats were killed by a schedule 1 method (Biomedical Science Unit, University of Birmingham) and the tendons teased out of their sheaths from the rat tails. Tendons were digested in 25 mL collagenase type I solution (1 mg/mL in PBS) and 15 mL trypsin solution (25 mg/mL in PBS) for 6 h at 37 °C with continuous stirring. After inactivation through the addition of 3 mL FBS, all tissue debris was filtered out using nylon gauze, and the suspension centrifuged at 3,000 rpm for 3 min. The cell pellet was resuspended in HAM's Nutrient Mixture (HAM, F12, Sigma Aldrich, UK) supplemented with 20 % v/v FBS (PAA, Germany) and 1 mM L-glutamine (Sigma Aldrich, UK). Cells were maintained in an incubator (MCO-15AC, Sanyo Electric Co. Ltd., UK) at 37 °C under an atmosphere of 5 % v/v CO_2 and 100 % relative humidity (RH); media were refreshed every 3 days.

2.8 Degradation studies

CaP discs were immersed and incubated in poly(styrene) 12 well plates of diameter 22 mm and height 20 mm (Scientific Laboratory Supplies, UK) stored in an incubator (MCO-15AC, Sanyo Electric Co. Ltd., UK) at a temperature of 37 °C under an atmosphere of 5 % v/v CO_2 and 100 % RH for up to 28 days. Day 0 represents 3 h after first immersion in solution. The unsupplemented media were (a) phosphate buffered saline (PBS, Sigma Aldrich, UK), (b) Dulbecco's Modified Eagle Medium (DMEM, Sigma Aldrich, UK), (c) HAM's Nutrient Mixture (HAM, F12, Sigma Aldrich, UK). The supplemented media were (d) DMEM supplemented with 10 % v/v FBS (S-DMEM), and (e) HAM supplemented with 20 % v/v FBS (S-HAM). Discs were immersed in 3 mL of cell culture media, which were either (i) unsupplemented and used as received, (ii) supplemented with FBS (PAA, Germany), (iii) neat FBS or dilutions thereof at 20 %, 40 %, 60 % and 80 % v/v, or (iv) S-HAM containing tenocytes at a concentration of $2.5x10^5$ cells/mL.

The media were refreshed every three days by first carefully removing the old media using a pipette, followed by gradual addition of fresh media around the disc until the liquid level was higher than the disc top surface and 3 mL of solution had been added. For tenocyte-seeded CaP discs, S-HAM supplemented with 1 mM L-glutamine was used for the media exchanges. All procedures were conducted under sterile conditions in a laminar flow hood (BSB 3-S, Gelaire ICN Biomedicals, UK).

2.9 Metabolic activity assay

3-(4,5-Dimethylthiazole-2-yl)-2,5-diphenyltetrazolium bromide (MTT, Sigma Aldrich, UK) was used to assess the metabolic activity of tenocytes and thus estimate the number of cells present. Firstly, 300 µL of MTT in PBS (25 mg/mL) was added to 3 mL of sample. Calibration plots were created to determine the amount of MTT required per disc, and the incubation time required, to obtain the maximum dissolution of MTT using 1:24 HCl/propan-2-ol. After 18 h incubation at 37 ^{o}C, 3 mL 1:24 HCl/propan-2-ol was added to the sample and incubated for a further 45 min at 37 ^{o}C. After repeated pipetting to ensure complete dissolution of formazan crystals, absorbance readings were taken in triplicate at a wavelength of 620 nm (Glomax Multi-detection system, Promega, UK) and used to calculate the number of metabolising cells present in each sample.

2.10 Statistical analysis

Data are presented in the format "mean ± standard error of the mean". Differences in mean values were compared within groups and significant differences were determined by define ANOVA (ANOVA) with post hoc Tukey-Kramer HSD (honestly significant difference) test. The significance level was set at $p< 0.05$.

3. Results

3.1 Structural morphology

The microstructure of the CaP samples was investigated using SEM; these results are shown in Fig. 1. It was found that whilst the TCP powder used for the printing process, a mixture of α- and β-TCP, showed the presence of irregular particles (Fig. 1A), the fractured samples (Fig. 1B) showed the presence of long blade-like crystals. These crystals are approximately 20 µm in length, exhibiting widths in the range 2-5 µm, which is the crystal morphology most frequently attributed to brushite [41].

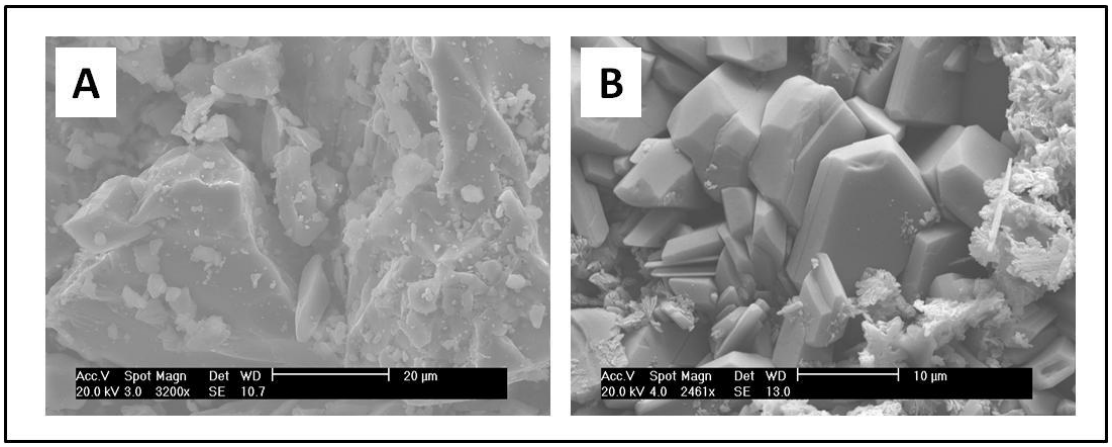

Fig. 1 SEM images of (A) the TCP powder used to manufacture the CaP discs and (B) the fracture surface of a printed CaP sample.

The crystal morphology of the CaP samples was inspected using SEM following immersion in PBS, DMEM, S-DMEM, HAM and S-HAM for up to 28 days. Fig. 2 shows the morphology of the surface of CaP samples after immersion in these media for 3 h (Fig. 2A-E) and 28 days (Fig. 2F-J). Fig. 2 shows that crystals of specimens aged in PBS become less defined after 28 days (Fig. 2A and F), with some roundness in crystal morphology seen. The morphological change in crystals immersed in DMEM and HAM show the presence of thin blade-like crystals after 28 days (Fig. 2G and I), whereas samples immersed in S-DMEM and S-HAM still retain crystal morphology similar to the Day 0 samples (Fig. 2H and J). The crystals in these samples appear to be coated by a secondary material of undefined structure.

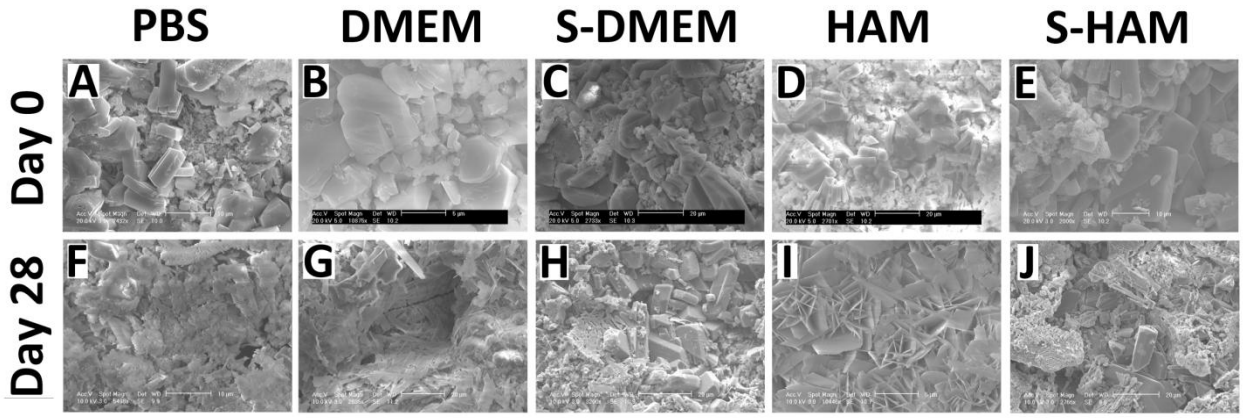

Fig. 2 SEM images of CaP scaffolds after immersion in PBS, DMEM, S-DMEM, HAM and S-HAM on Days 0 and 28. Scale bars in the images represent 5 µm (B, I), 10 µm (A, E, F) and 20 µm (C, D, G, H, J).

Fig. 3 shows SEM images obtained for tenocyte-seeded CaP scaffolds on Days 0-28. On Days 0, 3 and 7, (Fig. 3A-C) the tenocyte morphology is elongated which suggests surface attachment. By Day 14 onwards (Fig. 3D-F) ECM is present on the scaffold surface, whilst clearly defined tenocytes are no longer visible on the scaffold surface. The ECM can be seen to coat regions of the CaP crystals, for example on Days 21 and 28 (Fig. 3E-F). Uncoated crystals exhibit similar morphologies to those crystals visible post-immersion in acellular S-HAM, as shown in Fig. 2E and 2J.

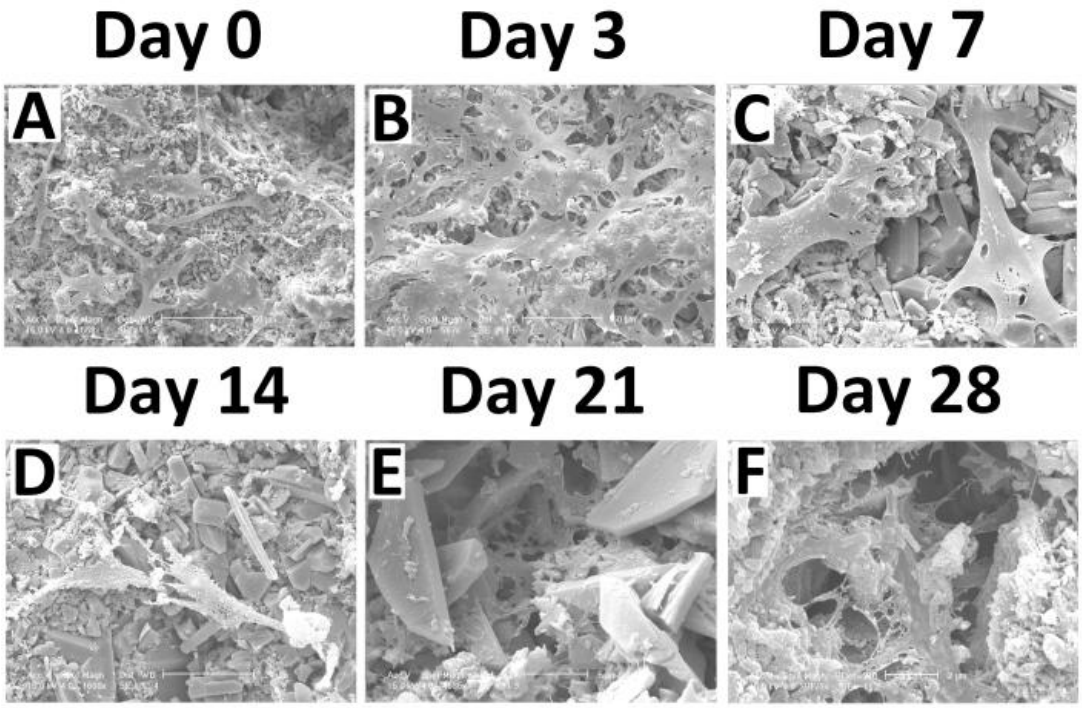

Fig. 3 SEM images of CaP scaffolds seeded with tenocytes on Days 0-28. Scale bars in the images represent 50 µm (A, B), 20 µm (C, D), 5 µm (E) and 2 µm (F).

Fig. 4 shows the effect of varying concentrations of FBS on the crystal morphology of CaP samples. It can be seen that crystal morphology changes dramatically for all concentrations of FBS used, as individual crystals become difficult to distinguish. The morphology appears significantly altered at FBS concentrations of 80 % and 100 % on all days. Although there are large pores visible in the CaP structure on Day 7 at FBS concentrations of 80 % and 100 %, the individual crystals on all days at the same concentrations appear smaller than those at lower concentrations. Of particular interest Fig. 4K shows a coating with similar morphology to that described for Fig. 2H and J.

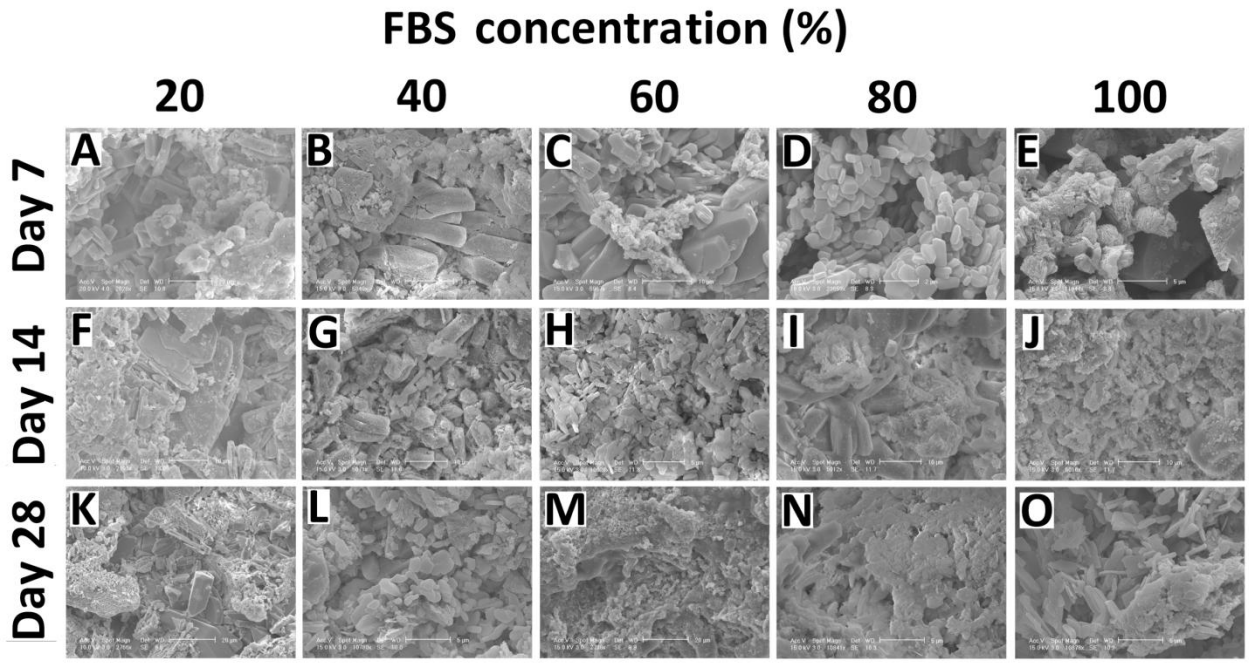

Fig. 4 Morphology of the surface of CaP scaffolds after immersion in FBS solutions of concentrations in the range 20-100 % (v/v), where 100 % represents neat FBS solution, used as received, whereas 20 % represents FBS solution at a dilution of 1/5. SEM images of the CaP scaffold surfaces are presented after immersion for 7 days (Fig. 4A-4E), 14 days (Fig. 4F-4J) and 28 days (Fig. 4K-4O). Scale bars in the images represent 2 µm (D), 5 µm (E, H, L, N, O), 10 µm (B, C, F, G, I, J) and 20 µm (A, K, M).

3.2 Surface roughness

The mean surface roughness of six CaP samples as manufactured was measured as 15.9 ± 2.0 µm. Fig. 5 shows the time-dependent change in surface roughness of CaP samples upon immersion in PBS (Fig. 5A), DMEM (Fig. 5B), S-DMEM (Fig. 5C), HAM (Fig. 4D) and S-HAM (Fig. 5E). Fig. 5F shows an example image of the surface topography of the CaP prior to immersion in dissolution media. Fig. 5A-C all show a significant decrease in surface roughness by Day 14. For Fig. 5A and 5B this is followed by an increase in roughness by Day 21 and a decrease in roughness by Day 28. Fig. 5D and 5E show similar surface roughnesses of all days studied. Here there is initially a rapid decrease in roughness on Day 0 followed by a gradual increase of surface roughness to a maximum by Day 14. This is followed by a decrease in roughness by Day 28. Fig. 5G shows the mean surface roughness of CaP scaffolds seeded with tenocytes on Days 0-28. It can be seen that there is no significant difference between the dry CaP disc and the seeded discs until Day 14. The surface roughnesses measured for CaP discs immersed in acellular S-HAM, shown in Fig. 5E, are comparable to the surface roughnesses presented here, for Days 7-28.

Fig. 5H shows the surface roughness of CaP samples immersed in FBS solutions of concentrations between 20-100 % v/v, where 100 % represents undiluted FBS solution used as received, whereas 20 % represents FBS solution at a dilution of 1/5. The roughness values show that there is no discernible trend in the effect of FBS concentration on the roughness of the CaP samples. There is a significant increase in the surface roughness of CaP samples submerged in 40 and 60% v/v FBS on Day 7 and Day 28. At higher concentrations there appears to be no significant effect.

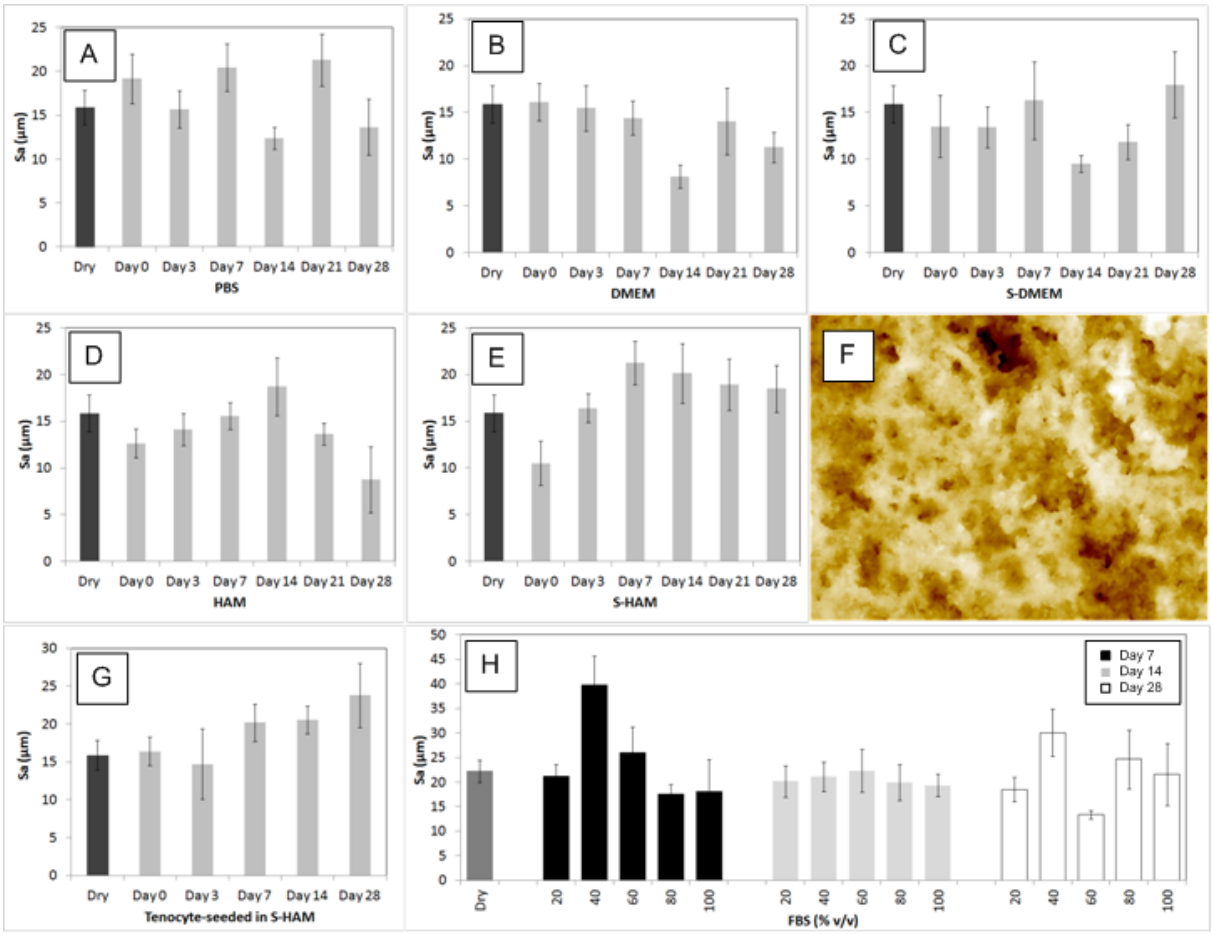

Fig. 5 Mean surface roughnesses of CaP scaffolds after immersion in (A) PBS, (B) DMEM, (C) S-DMEM, (D) HAM, and (E) S-HAM; (F) a representative image of the CaP surface prior to immersion; (G) mean surface roughnesses of tenocyte-seeded CaP scaffolds on Days 0-28; (H) mean surface roughnesses of CaP scaffolds immersed in 20 %, 40 %, 60 %, 80 % and 100 % v/v FBS on Days 7, 14 and 28 post-immersion.

3.3 Porosity and pore diameter distribution

Immersion in cell culture conditions affects not only the surface of the CaP samples, but also the internal structure and composition. Fig. 6A, 6C and 6E all show a representative pore diameter distribution of the dry CaP samples as measured using mercury porosimetry. The samples contained pore diameters covering three orders of magnitude, ranging from 10 nm to 10 µm, with a dominant peak at a pore diameter of approximately 100 nm. The porosity of the dry CaP samples, calculated using Eq. 1, given in §2.4, was found to be 35.9 ± 2.2 %.

Fig. 6A shows the pore diameter distributions of CaP samples immersed in PBS, DMEM, HAM, S-DMEM and S-HAM on Day 28. Fig. 6B shows the porosity of samples on Day 0, after 3 h immersion, and on Day 28. Fig. 6A shows that the pore diameters after 28 days immersion in unsupplemented media, PBS, DMEM and HAM, range between 10 nm- 1 µm, with the 100 nm peak which was prominent in the dry samples now significantly reduced in height. The majority of the pores on Day 28 lie in the range 10-100 nm. For these samples the maximum pore diameter is less than 10 µm. In comparison, samples immersed in the supplemented media, S-DMEM and S-HAM, exhibit no pores of diameter less than 1 µm, and pronounced peaks for pores of diameters in the range 1-5 µm. For these samples the maximum pore diameter is of the order 50 µm. Fig. 6B shows a significant increase in porosity for all samples immersed in cell culture media. The porosities for samples submerged in PBS, DMEM, S-DMEM and HAM increase from 35.9 % to 50-55 % after 3 h of immersion. Interestingly samples immersed in S-

HAM exhibited porosities of 64 % after 3 h. By Day 28 the porosities of all samples reached approximately 70 %.

Fig. 6C shows the pore diameter distributions of CaP scaffolds seeded with tenocytes on Days 0-28, whilst Fig. 6D shows the porosity of the scaffolds on Days 0-28. In Fig. 6C the pore diameters on Day 21 and Day 28 can be seen to be greatly reduced from those measured for the dry CaP scaffold. In Fig. 6D it can be seen that the porosity of the scaffold does not change significantly from that of the dry scaffold over the 28 day period studied. Scaffolds immersed in acellular S-HAM (Fig. 6B) exhibited approximately 70 % porosity on Day 28, which is almost twice the porosity exhibited for the scaffolds seeded with tenocytes and incubated in S-HAM, as presented here; this point is discussed further in §4.3.

Pore diameter distribution data collected for samples immersed in increasing concentrations of FBS, shown in Fig. 6E, reveal that for 20 % v/v FBS the pore diameter distribution after 28 days is similar to those exhibited by samples immersed in supplemented media, as shown in Fig. 6A. It should be noted that S-DMEM contains 10 % v/v FBS whilst S-HAM contains 20 % v/v FBS. For FBS concentrations of 40 % v/v and greater it is apparent that the dominant 100 nm peak present in the dry samples is retained after 28 days. Pores of diameter less than 100 nm are also increasingly apparent as the FBS concentration is increased. From the porosity data shown in Fig. 6F, a significant increase in porosity is seen after a 3 h immersion in FBS. Regardless of the concentration of FBS all samples exhibit porosities in the range 60-65 % after 3 h. By Day 28 samples immersed in 40 % v/v FBS and above exhibited porosities between 60-70 % whilst samples immersed in 20 % v/v FBS exhibited the greatest porosity of 72 %.

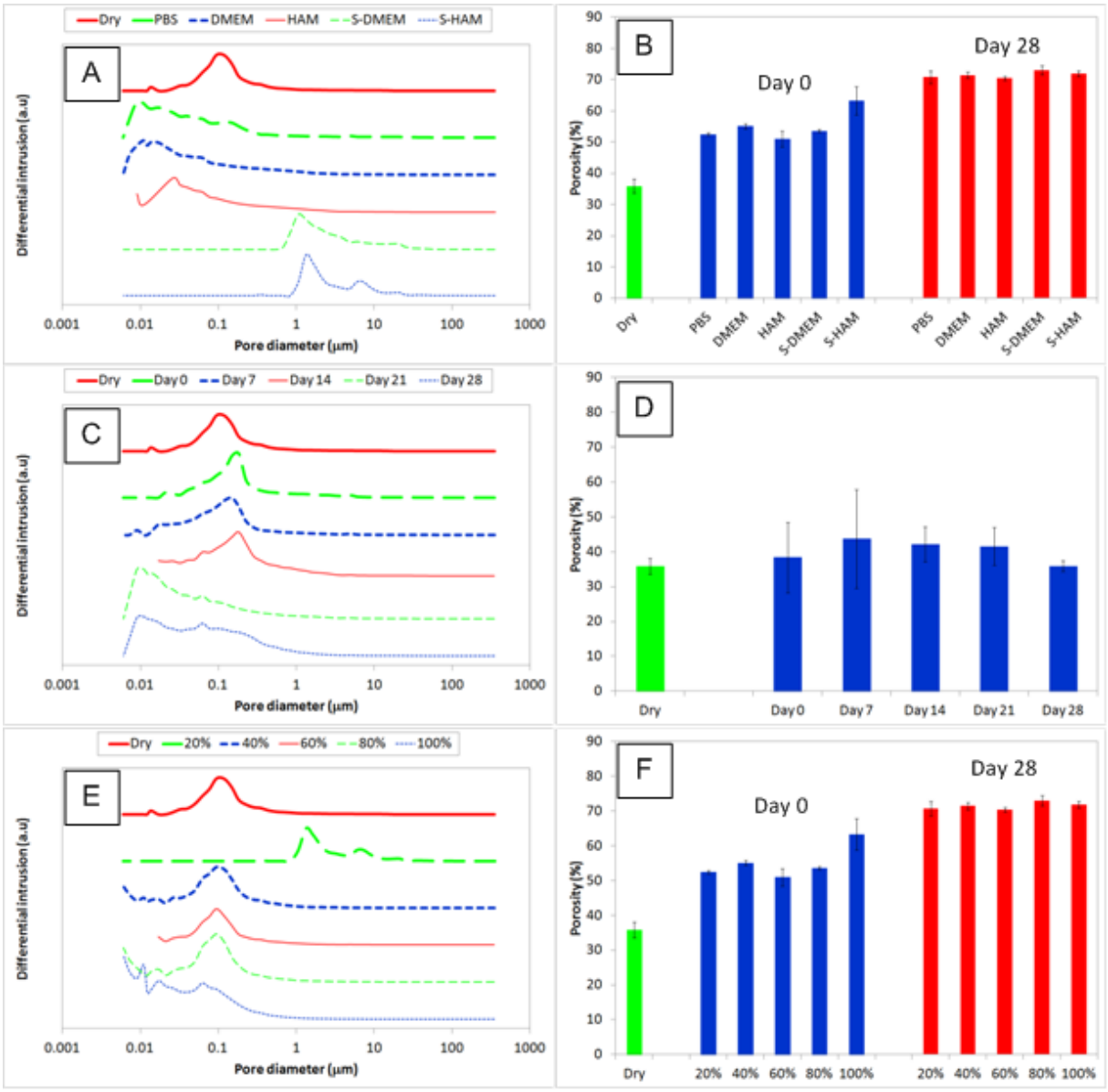

Fig. 6 (A) Pore diameter distribution of CaP scaffolds immersed in PBS, DMEM, HAM, S-DMEM and S-HAM on Day 28, and (B) calculated porosity of CaP scaffolds immersed in PBS, DMEM, HAM, S-DMEM and S-HAM on Day 0 and Day 28; (C) pore diameter distribution of CaP scaffolds seeded with tenocytes on Days 0-28 and (D) calculated porosity of CaP scaffolds seeded with tenocytes on Days 0-28; (E) Day 28 pore diameter distribution and (F) Day 0 and Day 28 calculated porosities of CaP scaffolds immersed in 20 %, 40 %, 60 %, 80 % and 100 % v/v FBS.

3.4 X-ray diffraction

Fig. 7 shows the XRD patterns obtained for CaP scaffolds following immersion for 28 days in unsupplemented media (B, C, E), supplemented media (D, F), and 20, 60, and 100 % v/v FBS (G-I). Fig. 7A shows the XRD patterns for the TCP powder prior to 3D printing, and the CaP scaffold post-hardening in phosphoric acid. The latter pattern represents the initial composition for all subsequent studies. After immersion for 28 days in the various media, the XRD patterns obtained revealed that no significant change in chemical composition was discernible. One slight exception to this can be seen in Fig. 7E, where a new peak is clearly visible at $2\theta = 22.8^{\circ}$ which is believed to correspond to a Cu-containing compound; HAM is the only media studied here which contains Cu ions. Comparison with Fig. 7F reveals that the equivalent peak is not present for CaP immersed in FBS-supplemented HAM. Similarly, the equivalent peak is not present for CaP immersed in any other of the media studied here.

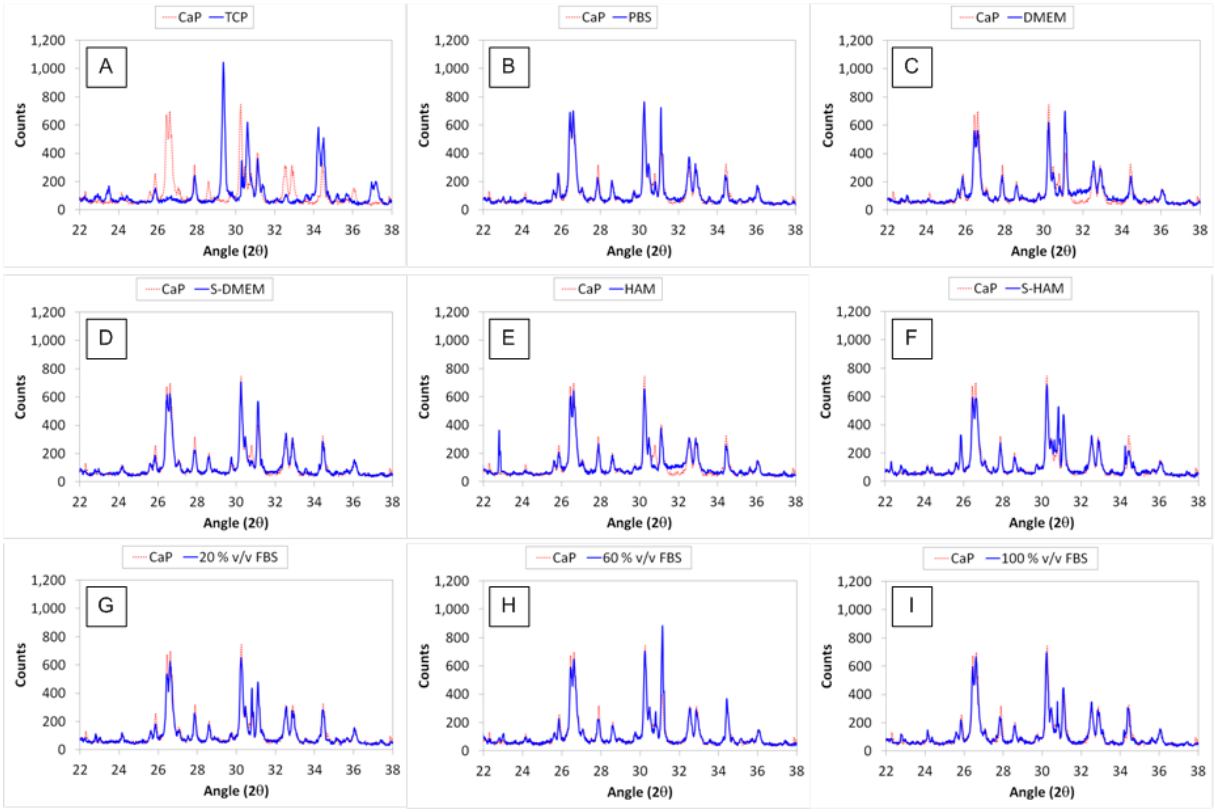

Fig. 7 X-ray diffraction patterns for (A) TCP pre-printing and CaP scaffolds post-hardening, and for CaP scaffolds after immersion in (B) PBS, (C) DMEM, (D) S-DMEM, (E) HAM, (F) S-HAM, (G) 20 % v/v FBS, (H) 60 % v/v FBS, and (I) 100 % v/v FBS.

3.5 Metabolic activity assays

Fig. 8(A) shows the metabolic activity of tenocytes over a 30 day period, in which data a plateau (Day 2-20) and subsequent death phase (Day 20-30) can be seen. In comparison, Fig. 8(B) shows the metabolic activity of tenocytes seeded on CaP scaffolds on Days 0-28. A decline in the number of tenocytes can be seen from Day 7 onwards in Fig. 8(B), which is contrary to the growth curve shown in Fig. 8(A), as this shows that tenocytes are still in the plateau phase at this time.

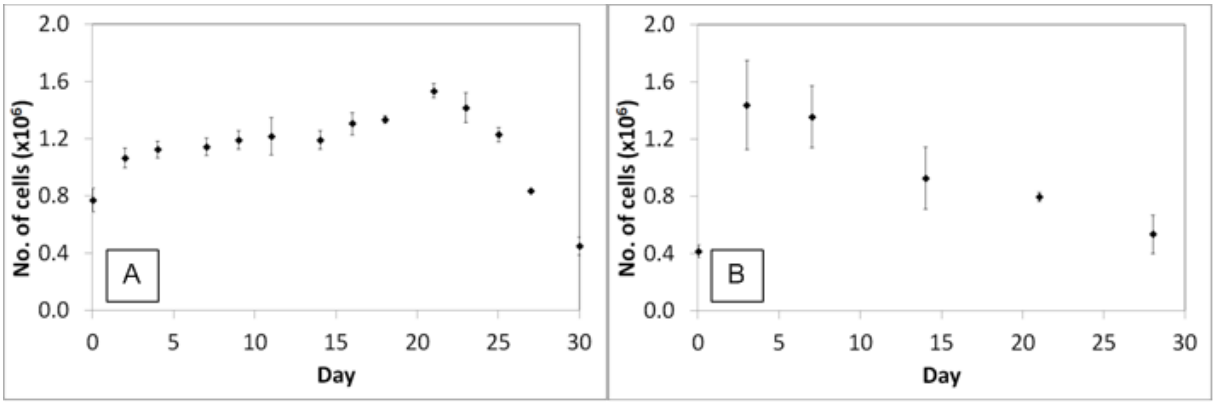

Fig. 8 (A) Tenocyte life cycle represented by metabolic activity and (B) metabolic activity of tenocytes seeded on CaP scaffolds on Days 0-28 post-immersion.

4. Discussion

4.1 Effect of immersion in unsupplemented media on CaP discs

The results show that immersion in cell culture media causes pronounced changes to the porosity, crystal morphology and surface roughness of CaP discs, but no distinguishable pattern of change in their chemical composition, as evidenced by XRD (Fig. 7). However, the presence of a peak at 22.8 ^{o} in the pattern obtained for CaP immersed in HAM was not matched by the presence of an equivalent peak in the pattern for CaP immersed in FBS-supplemented HAM. This peak indicates a reprecipitation process occurring for CaP immersed in HAM. Therefore the absence of the peak for CaP immersed in S-HAM could be indicative of FBS inhibiting reprecipitation of material from solution. Significant further work is required in order to elucidate this phenomenon in greater detail; such work is beyond the scope of the research presented here. Immersion in the unsupplemented media PBS, DMEM and HAM led to a significant increase in porosity after 28 days, shown in Fig. 6, with discs exhibiting pore diameters equal to and smaller than those exhibited by the discs immediately after manufacture. Previously published research on scaffolds printed in this way, using the same raw materials, suggests the presence of monetite within the structures. It was reported that hydrothermal conversion of brushite to monetite led to an increase in porosity of approximately 13 % [42]. Although monetite formation was not detected in the work presented here, the increase in porosity is suggestive of CaP dissolution, a process which may or may not reach equilibrium before the media are refreshed every 3 days. Further discussion of the importance of refreshing the media can be found in §4.4.

The appearance of small pores after 28 days immersion, which were not present in as great a quantity in the disc prior to immersion, is also suggestive of dissolution. However, the change in crystal morphology, shown in Fig. 2, and the non-appearance of pores of larger diameter than those found in the disc prior to immersion, is suggestive of reprecipitation of dissolved material. Work conducted by Constantz *et al.* [43] showed via Fourier transform Infrared spectroscopy that HA forms on brushite crystals after just 72 h immersion in PBS. However, it is unclear whether the reprecipitation is HA or an intermediate phase, such as octacalcium phosphate as evidenced by Temizel *et al.* [44] as this was not investigated by Constantz *et al.* [43] in their study of brushite powder at 37˚C. The change in CaP disc surface roughness as a function of time, shown in Fig. 4, indicates that morphological changes in disc structure are occurring, which would have implications for the incorporation of cells into this synthetic hard tissue matrix. Further discussion of this point can also be found in §4.4.

It is possible that the continual change in surface roughness with immersion time is the gradual revealing of the underlying 3D structure of the discs, as created during manufacture, with surface layers being dissolved, thus continually providing new surface morphologies. Passive resorption by chemical dissolution can occur if there is a fluctuation of ion concentrations from the solubility products to the surrounding solution. The degradation of CaP may be controlled by adding magnesium or pyrophosphate ions to the cement matrix [34] under which conditions it is thought that the ions adsorb to HA crystal nuclei and block active growth sites [45-46]. However, evidence also exists of previously believed inhibitors of crystal formation acting as promoters under certain conditions, i.e. when adsorbed onto a solid substrate in a certain orientation [47].

4.2 Effect of immersion in supplemented media on CaP discs

Immersion in the supplemented media S-DMEM and S-HAM lead to a significant increase in porosity after 28 days, with the majority of pore diameters approximately one order of magnitude larger than those exhibited by the discs immediately after manufacture and maximum pore diameters approximately two orders of magnitude larger; these results are shown in Fig. 6. The initial increase in

porosity occurs more rapidly for discs immersed in S-HAM than in S-DMEM, which can be explained by the difference in FBS composition of the two media; 10 % v/v for S-DMEM and 20 % v/v for S-HAM. The analogous result was not observed for discs immersed in the unsupplemented HAM and DMEM, also shown in Fig. 6. Immersion in supplemented media yielded crystals which appeared smaller than those visible following immersion in unsupplemented media; these results can be seen in Fig. 2-3. There also appeared to be small fragments of material exhibiting a non-crystalline morphology coating the crystals; this is attributed to adsorbed protein, to which a number of researchers have previously made reference [48]. Immersion in 20 % v/v FBS solution yielded a similar change in porosity as did immersion in S-DMEM and S-HAM, which contained 10 % v/v and 20 % v/v FBS respectively; a rapid increase in porosity accompanied by an order of magnitude increase in the dominant pore diameters, as shown in Fig. 6. It has previously been suggested that brushite hydrolysis may be inhibited on FBS immersed samples [34]. Protein adsorption on the crystal surfaces could prevent the formation of HA, and therefore it is likely that new pores can be formed via the dissolution of brushite, although adsorbed proteins will act as a diffusion barrier and if the previously mentioned studies by Addadi *et al.* [47] are taken into account, the presence of a complex protein solution could both inhibit and promote HA nucleation. Immersion in 40-100 % v/v FBS solutions similarly yielded rapid increases in porosity, but significantly different pore diameter distributions. Pores of diameter larger than those found in the disc prior to immersion were not apparent, whilst a range of pores of diameters from 10-100 nm and smaller were created by Day 28.

4.3 Effect of tenocyte seeding on CaP discs

The elongated tenocyte morphology visible in the SEM images of tenocyte-seeded CaP scaffolds (Fig. 3A-C) indicates attachment of tenocytes to the scaffold. Tenocyte morphology is less visible on Days 14-28 (Fig. 3D-F) and the metabolic activity assay (Fig. 8B) indicates that the number of viable tenocytes present on or within the scaffold is decreasing by this time. Therefore, it can be assumed that the material which can be seen in the SEM images (Fig. 3E-F) to coat the CaP crystals is ECM. Such material is not visible in the SEM images for CaP scaffolds immersed in acellular S-HAM (Fig. 2E and J). Whilst the crystal morphology is difficult to define due to ECM production, the crystals that are visible (Fig. 3E-F) exhibit defined structures similar to the CaP scaffolds immersed in acellular S-HAM on Day 0 (Fig. 2E), but not on Day 28 (Fig. 2J). This suggests that crystal dissolution is inhibited by the production of ECM. This is supported by similar porosities exhibited by dry CaP scaffolds and those seeded with tenocytes after 28 days (Fig. 10B), which did not occur for CaP scaffolds immersed in acellular S-HAM. On the contrary, these scaffolds exhibited a rapid increase in porosity after only 3 h (Fig. 6B). There is a reduction in pore diameters on Day 21 and 28 (Fig. 6C), which could be attributed to the adsorption of ECM proteins onto the existing pore surfaces. In order to investigate this further, a matrix quantification assay, such as the glycosaminoglycan (GAG) assay, could be employed. This is a topic currently under consideration for future work. The roughness of the CaP scaffold surface on Day 28 was comparable for scaffolds immersed under both the cellular and acellular conditions. For the cellular conditions, this result is attributable to a lack of dissolution of the CaP and the gradual accumulation of adsorbed ECM and adhered tenocytes. In contrast, for the acellular conditions, the measured increase in porosity shows that dissolution and removal of material by attrition is occurring. Hence, the similar surface roughnesses are believed to be an artefact of the layer-by-layer printing process.

4.4 Relevance to in vitro *and* in vivo *studies*

One of the main advantages of 3D printing CaP scaffolds is not only the reproducibility but that individual wound geometries in a clinical application may be catered for. This is of particular relevance to situations where the defect is irregularly shaped and is not something which may be achieved easily

through hand-cast methods. However, the scaffold changes highlighted in this study in *in vitro* conditions may still considerably influence their use *in vivo*. Specifically the change in CaP scaffold surface roughness as a function of time in acellular conditions, shown in Fig. 4, indicates that morphological changes in disc structure occur rapidly upon immersion, and continue to occur over the 28 day duration of the study performed here. In contrast, the presence of tenocytes and the production of ECM appeared to inhibit dissolution and morphological changes to the CaP scaffold. This result has implications for the time at which cells are introduced to the synthetic hard tissue matrix. It is conceivable that with careful selection of a preconditioning period, during which time the scaffold is immersed under acellular conditions, a target scaffold porosity could be achieved. The addition of cells would then serve to inhibit further dissolution of the scaffold. However, it should be noted that this result currently holds true only for tenocytes, and extensive further work is required before this result could be extrapolated to other cell types.

For cellular samples it is necessary to change the media every three days, or possibly more frequently than this, depending on the cell type. Frequent media exchange serves to disturb any equilibrium which has either been created between the solid and liquid phases, or is in the process of being established. Hence, through a combination of dissolution and disintegration caused by mechanical agitation due to shear stresses introduced during fluid exchange [49], the scaffold on which cellular growth is desired can be considerably altered. Such a result may be beneficial, particularly in those systems where cell growth and proliferation leads to increases in cell population over time. Understanding the internal pore diameters of matrices is essential for modelling cellular migration and proliferation, and the diffusion of both dissolved nutrients and toxic by-products of cellular growth within the matrix. The total surface area for attachment is increased by the presence of pores, either through expansion of existing pores or the development of new pores, and hence there is greater chance of attachment of the scaffold to the native bone *in vivo* [50]. Large pores of diameter 100-200 μm are suitable for bone integration whilst smaller pores of diameter 10-75 μm are ideal for soft tissue penetration [50]. In particular pore sizes of 100-500 nm affect bone resorption [51] whilst pore sizes of 1.2-2.0 μm allow for better cellular migration and facilitate new tissue formation [52]. Increased porosity is a favourable outcome of immersion since *in vivo* osteogenesis is induced by porous ceramics, with non-porous ceramics shown not to contribute to new bone formation [53]. However, whilst this may be ideal for cellular migration and native tissue integration, the porosity change is also likely to cause significant changes to the mechanical integrity of the scaffold. Depending upon the chosen solution conditions, the presence of surface HA may stabilise matrices *in vivo* against further dissolution. It has previously been reported that spontaneous growth of apatite can occur *in vivo* once nucleation begins [54], although it should be noted that nucleation of HA and growth of existing HA are two different classes of study [55]. Matrix stability against dissolution may not be ideal in those situations where a controlled degradation rate is necessary in order to allow growth of new tissue, but it may be possible to pause and continue matrix dissolution at specified times via careful selection of cell culture media.

5. Conclusion

The effect of prolonged immersion times *in vitro* on the degradation and stability of 3D printed calcium phosphate scaffolds has been investigated. The scaffolds were incubated in a range of acellular culture media for up to 28 days. Dissolution was found to occur, evidenced by changes in crystal morphology and increases in scaffold porosity; no change in chemical composition was observed. Fluctuations in surface roughness suggested sequential removal of the exterior printed layers. Scaffolds seeded with tenocytes did not exhibit such behaviour; tenocytes were found to adhere to the scaffold, depositing ECM which inhibited scaffold degradation. Media supplemented with foetal bovine serum and incubated for 28 days induced a rapid increase in scaffold porosity with pore diameters 1-2 orders of magnitude larger than pores present immediately post manufacture. The appearance of small crystals which were coated in an amorphous material suggested protein adsorption was occurring within the scaffold. Higher concentrations of sera proteins yielded pores with diameters in the range 10-100 nm and below, which was not observed in media with serum concentrations less than 40 % v/v.

These results highlight the complexities and possible benefits associated with using calcium phosphates for *in vitro* and *in vivo* studies, whereby the scaffold exhibits dynamic properties as a result of interactions with the surrounding medium. This research highlights the dynamic nature of calcium phosphate based bone scaffolds in tissue culture conditions which may be complicated further *in vivo* by the complexity of the environment.

Acknowledgements
The helium pycnometer, interferometer and mercury porosimeter used in this research were obtained through Birmingham Science City: Innovative Uses for Advanced Materials in the Modern World (West Midlands Centre for Advanced Materials Project 2), with support from Advantage West Midlands (AWM) and part funded by the European Regional Development Fund (ERDF). The authors would like to thank Mr Paul Stanley and Mrs Theresa Morris in the Centre for Electron Microscopy at the University of Birmingham. The authors would also like to thank Mrs Elaine Mitchell in the School of Biochemical Engineering at the University of Birmingham for technical support.

Supporting Information
Raman spectroscopic analysis of scaffolds is available as supporting information.

References
1. A. Sogal and A.J. Tofe, J. Periodontal, 70 (1999) 1053.
2. M. Fröhlich, W.L. Grayson, L.Q. Wan, D. Marolt, M. Drobnic and G. Vunjak-Novakovic, Curr. Stem Cell Res. Ther., 3 (2008) 254.
3. M. Gabl, C. Reinhart, M. Lutz, G. Bodner, A. Rudisch, H. Hussland S. Pechlaner, J. Bone Joint Surg., 81 (1999) 1414.
4. A. Matsuno, H. Tanaka, H. Iwamuro, S. Takanashi, S. Miyawaki, M. Nakashima, H. Nakaguchi and T. Nagashima, Acta Neurochir., 148 (2006) 5350.
5. J.P. Becktor, H. Hallström, S. Isaksson and L. Sennerby L, J. Oral Maxillofac. Surg., 66 (2008) 780.
6. H. Seitz, W. Rieder, S. Irsen, B. Leukers and C. Tille, J. Biomed. Mater. Res. B, 74 (2005) 782.
7. C.R. Jacobs, J. Rehabil. Res. Dev., 37 (2000) 209.
8. D.J. Hadjidakis and I.I. Androulakis, Ann. N.Y. Acad. Sci., 1092 (2006) 385.
9. J.R. Porter, T.T. Ruckh and K.C. Popat, Biotech. Prog., 25 (2009) 1539.
10. J.S. Silber, D.G. Anderson, S.D. Daffner, B.T. Brislin, J.M. Leland, A.S. Hilibrand, A.R. Vaccaro and T.J. Albert, Spine, 28 (2003) 134.
11. F. Cahn, J. Regen. Med., 1 (2000) 145.
12. C.T. Laurencin and S.F. El-Amin, J. Am. Acad. Orthop. Surg., 16 (2008) 4.
13. P. Habibovic and J.E. Barralet, Acta Biomat., 7 (2011) 3013.
14. F. Tamimi, Z. Sheikh and J.E. Barralet, Acta Biomat., 8 (2012) 474.
15. Y. Takahashi, M. Yamamoto and Y. Tabata, Biomat., 26 (2005) 4856.
16. H. Yoshikawa and A. Myoui, J. Artific. Organs., 8 (2005) 131.
17. M.W. Laschke, A. Strohe, M.D. Menger, M. Alini and D. Eglin, Acta Biomat., 6 (2010) 2020.
18. H. Zhou and J. Lee, Acta Biomat., 7 (2011) 2769.
19. B. Duan, M. Wang, W.Y. Zhou, W.L. Cheung, Z.Y. Li and W.W. Lu, Acta Biomat., 6 (2010) 4495.
20. G. Wei and P.X. Ma, Biomat., 25 (2004) 4749.
21. H. Aoki, K. Kato, M. Ogiso and T. Tabata, J. Dent. Eng., 18 (1977) 86.
22. M. Bohner, U. Gbureck and J.E. Barralet, Biomat., 26 (2005) 6423.
23. K.A. Gross and C.C. Berndt, Mineralog. Soc. Am., (2002) 631.
24. H.N. Lim, N.M. Huang, M.A. Yarmo, P.S. Khiew and W.S. Chiu, Colloid J., 71 (2009) 793.
25. S. Pina and J-M.F. Ferreira, Mat., 3 (2010) 519.
26. A.R. Calafiori, G. Di Marco and G. Martino, J. Mater. Sci. Mater. Med., 18 (2007) 2331.
27. E. Sachlos and J.T. Czernuszka, Eur. Cells Mater., 5 (2008) 29.
28. P.J.S. Bartolo, H. Almeida and T. Laoui, Int. J. Comp. App. Tech., 36 (2009) 1.
29. J.Y. Kim, T-J. Lee, D-W. Cho and B-S. Kim, J. Biomat. Sci., 21 (2010) 951.
30. A.J. Salgado, O.P. Coutinho and R.L. Reis, Macromol. Biosci., 4 (2004) 743.

31. D.W. Hutmacher, Biomat., 21 (2000) 2529.
32. U. Klammert, E. Vorndran, T. Reuther, F.A. Müller, K. Zorn and U. Gbureck, J. Mater. Sci. Mater. Med., 21 (2010) 2947.
33. E. Vorndran, U. Klammert, A. Ewald, J.E. Barralet and U. Gbureck, Advan. Func. Mater., 20 (2010) 1585.
34. L.M. Grover, U. Gbureck, A.J. Wright, M. Tremayne and J.E. Barralet, Biomat., 27 (2006) 2178.
35. P. Liu, J. Tao, Y. Cai, H. Pan, X. Xu and R. Tang, J. Cryst. Growth, 310 (2008) 4672.
36. S. Bertsch and F. Marks, Nature, 251 (1974) 517.
37. C.D. Gerharz, H.E. Gabbert, H.K. Biesalski, R. Engers and C. Luley, Brit. J. Cancer, 59 (1989) 61.
38. M. Sallot, I. Lascombe, L. Bermont and M. Jouvenot, Anticancer Res., 17 (1997) 3499.
39. M.I. Naseer, H. Zubair, Ikramullah and M.O. Kim, Pak. J. Med. Sci., 25 (2009) 500.
40. N. Mehrban, J.Z. Paxton, J. Bowen, E. Vorndran, U. Gbureck and L.M. Grover, Advan. in Appl. Ceram., 110 (2011) 162.
41. M. Bohner, J. Lemaitre and T.A. Ring, J. Am. Ceram. Soc., 79 (1996) 1427.
42. U. Gbureck, T. Hölzel, U. Klammert, K. Würzler, F.A. Müller and J.E. Barralet, Advan. Funct. Mat., 17 (2007) 3940.
43. B.R. Constantz, B.M. Barr, I.C. Ison, M.T. Fulmer, J. Baker, L.A. McKinney, S.B. Goodman, S. Gunasekaren, D.C. Delaney, J. Ross and R.D. Poser, J. Biomed. Mater. Res., 43 (1998) 451.
44. N. Temizel, G. Girisken and A.C. Tas, Mater. Sci. Eng. C, 31 (2011) 1136.
45. Z. Amjad, P.G. Koutsoukos and G.H. Nancollas, J. Colloid. Interf. Sci., 101 (1984) 250.
46. N. Eidelman, W.E. Brown and J.L. Meyer, J. Cryst. Growth, 113 (1991) 643.
47. L. Addadi, J. Moradian-Oldak, H. Füredi-Milhofer, S. Weiner, A. Veis in H. Slavkin and P. Price (Eds.), Chemistry and biology of mineralized tissues. Excerpta Medica, Elsevier, Amsterdam, 1992, 153.
48. J.L. Giocondi, B.S. El-Dasher, G.H. Nancollas and C.A. Orme, Philos. Trans. R. Soc. A. Math. Phys. Eng. Sci., 368 (2010) 1937.
49. L.M. Grover, J.C. Knowles, G.J.P. Fleming and J.E. Barralet, Biomat., 24 (2003) 4133.
50. V. Karageorgiou and D. Kaplan, Biomat., 26 (2005) 5474.
51. H. Yokozeki, T. Hayashi, T. Nakagawa, H. Kurosava, K. Shibuya and K Ioku, J. Mat. Sci: Mat. in Med., 9 (1998) 381.
52. C.E. Holly, M.S. Schoichet and J.E. Davies, J. Biomed. Mater. Res., 51 (2000) 376.
53. H. Yuan, K. Kurashina, J. de Bruijn, Y. Li, K. de Groot and X. Zhang, Biomat., 20 (1999) 1799.
54. A.C. Tas, Biomat., 21 (2000) 1429.
55. E. Mueller and C.S. Sikes, Calc. Tissue Int., 52 (1993) 34.